

Molecular beam epitaxy growth of the highly conductive oxide SrMoO₃

Hiroshi Takatsu,¹ Naoya Yamashina,¹ Daisuke Shiga,^{2,3} Ryu Yukawa,² Koji Horiba,² Hiroshi Kumigashira,^{2,3} Takahito Terashima,⁴ and Hiroshi Kageyama¹

¹*Department of Energy and Hydrocarbon Chemistry,
Graduate School of Engineering, Kyoto University, Kyoto 615-8510, Japan*

²*Photon Factory, Institute of Materials Structure Science,
High Energy Accelerator Research Organization (KEK), 1-1 Oho, Tsukuba 305-0801, Japan*

³*Department of Physics, Tohoku University, Sendai 980-8578, Japan*

⁴*Department of Physics, Graduate School of Science, Kyoto University, Kyoto 606-8502, Japan*

(Dated: December 7, 2020)

SrMoO₃ is a promising material for its excellent electrical conductivity, but growing high-quality thin films remains a challenge. Here we synthesized epitaxial films of SrMoO₃ using molecular beam epitaxy (MBE) technique under low oxygen-flow rate. Introduction of SrTiO₃ buffer layers of 4–8 unit cells between the film and the (001)-oriented SrTiO₃ or KTaO₃ substrate was crucial to remove impurities and/or roughness of the film surface. The obtained film shows improved electrical conductivities as compared with films obtained by other techniques. The high quality of the SrMoO₃ film is also verified by angle resolved photoemission spectroscopy (ARPES) measurements showing a clear Fermi surfaces.

I. INTRODUCTION

Perovskite oxides with a general formula ABO_3 exhibit various intriguing properties such as ferroelectricity, piezoelectricity, ion conductivity, colossal magnetoresistance, and superconductivity¹. SrMoO₃ is a Pauli paramagnetic metal with excellent electrical conductivity^{2,3}. The room temperature (RT) resistivity ρ of single-crystalline SrMoO₃ is as low as $5 \mu\Omega \text{ cm}$, which is much lower than typical oxide materials⁴ and is rather close to those of nearly free electron systems such as sodium and copper. The utmost feature of this oxide has stimulated intensive studies to grow epitaxial films^{5–9} for applications, for example, electrodes between oxide interfaces^{5,10} and transparent conductors^{6,11}. Unfortunately, all the films, so far prepared by pulsed laser deposition (PLD)^{7–12} or sputtering^{5,6}, show rather poor resistivity ($27\text{--}150 \mu\Omega \text{ cm}$) than that of the bulk single crystal, possibly due to the presence of defects or inclusion of impurity phases. It is notable that an insulating Mo⁶⁺ phase is often found in the surface state^{10–12}.

Among available techniques of thin film preparation, molecular beam epitaxy (MBE) is known as a method that allows the growth of thin films with high quality¹³. This is because much smaller kinetic energy of constituent elements supplied in this process¹⁴ provides an almost thermal equilibrium condition, avoiding an undesired oxide off-stoichiometry. For this reason, we have employed the MBE method, for the first time, to grow SrMoO₃ films, using elemental Sr and Mo as fluxes. By optimizing growth conditions such as O₂ flow rate, we have successfully obtained epitaxial thin film of SrMoO₃. In particular, the use of a SrTiO₃ buffer layer between the SrMoO₃ film and the substrate is found to be crucial to obtain high quality films with less impurities and/or roughness in the surface. The high-quality of the film is verified by X-ray diffraction (XRD) and angle resolved photoemission spectroscopy (ARPES) measure-

ments. The film with the SrTiO₃ buffer layer exhibited an improved resistivity of $24 \mu\Omega \text{ cm}$ at RT as compared with the SrMoO₃ films by other techniques^{5,7–9,11,15,16}.

II. EXPERIMENTAL SECTION

Films of SrMoO₃ were grown on the (001)-oriented SrTiO₃ (STO) or KTaO₃ (KTO) substrates with a custom-made reactive MBE system (EGL-1420-E2, Biemtron). Elemental Sr and Mo fluxes were simultaneously provided from a conventional Knudsen cell and electron beam evaporation system. Typical flux rates were 0.04 \AA/s for Sr and 0.01 \AA/s for Mo, as determined by an INFICON quartz crystal microbalance system before growth. The growth temperature window was $450\text{--}600 \text{ }^\circ\text{C}$, which was monitored by an optical pyrometer. The optimal growth temperature was found to be $520 \text{ }^\circ\text{C}$. We flowed O₂ gas at a rate of 0.1 sccm , which gives a background pressure of about $4 \times 10^{-7} \text{ Torr}$. Lower quality SrMoO₃ films were obtained under a higher oxygen pressure, while under ozone flow, SrMoO₃ was not obtained. The surface structure of the film and substrate was monitored *in-situ* by reflection high-energy electron diffraction (RHEED) with an acceleration voltage of 20 keV .

X-ray diffraction (XRD) measurements after the growth were carried out at RT with a Rigaku SmartLab diffractometer equipped with a Cu K α_1 monochromator.

The electrical resistivity ρ was measured by using a standard four-probe method. Au/Ti metal electrodes were vacuum-evaporated on the films for electrical contacts, and gold wires ($\phi = 30 \mu\text{m}$) were attached with silver paste to these electrodes.

Soft x-ray photoemission measurements were performed at $T = 20 \text{ K}$ with a synchrotron-radiation photoemission spectroscopy system at Photon Factory BL-2. The film used in these measurements was deposited after

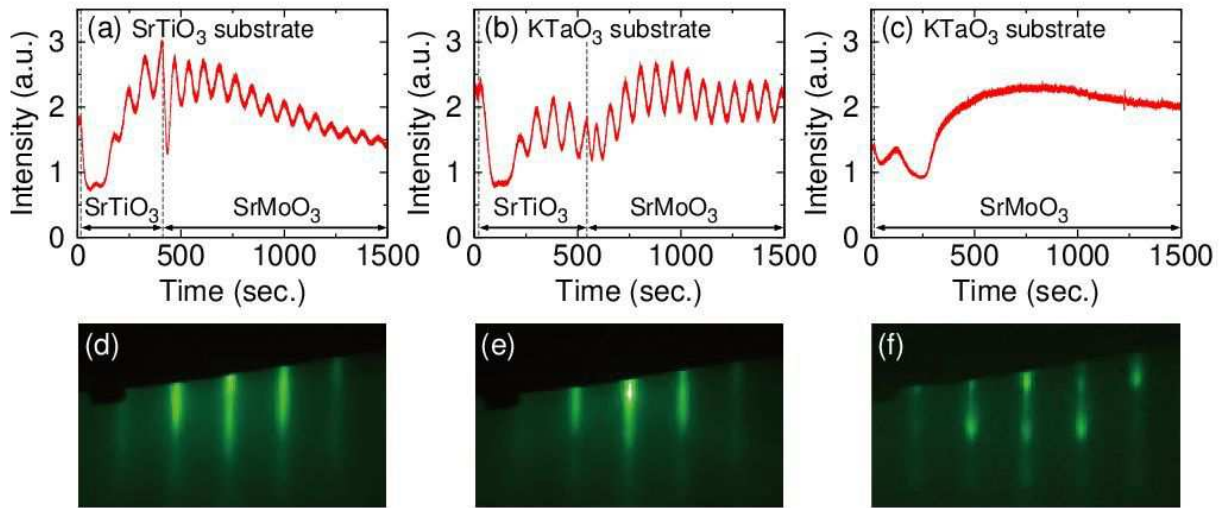


FIG. 1. RHEED intensity oscillations during deposition of SrMoO₃ film and SrTiO₃ (STO) buffer layer on (a) the Nb-doped (001)-STO substrate and (b) the (001)-KTO substrate. (c) RHEED intensity oscillations during deposition of SrMoO₃ film on the (001)-KTO substrate. (d)-(f) RHEED images along [100] of the STO (or KTO) substrate for the same samples in (a)-(c), respectively.

the growth of a STO buffer layer on the Nb-doped (001)-STO substrate to eliminate the charging effect. The thickness of the SrMoO₃ film used in experiments was 14.6 nm. The top of the film was capped with one unit cell of STO to protect the SrMoO₃-film surface from further oxidation. Thus no surface cleaning was conducted. ARPES was performed for the same sample. The position of Fermi energy E_F was determined by measuring the spectra of gold which was electrically connected to the sample.

For the theoretical reference of ARPES results, electronic structures were calculated using the QUANTUM ESPRESSO package^{17,18}. We used projector-augmented wave pseudopotentials¹⁹ and the Perdew-Burke-Ernzerhof parameterization of the generalized gradient approximation²⁰. The cutoff energies in the wave function and charge densities were 80 and 500 Ry, respectively. A $10 \times 10 \times 10$ k -mesh in the first Brillouin zone was used. It is worth noting that the bulk SrMoO₃ exhibits structural transitions, upon heating, from an orthorhombic phase to a tetragonal phase at $T = 150$ K, and to a cubic phase at 250 K²¹. However, the distortion from the cubic symmetry is subtle and does not largely alter its band structure¹². Our band structure calculations also confirmed this result. We will show the result for the cubic SrMoO₃ unless otherwise specified.

III. RESULTS AND DISCUSSION

For the growth of high quality SrMoO₃ films, we used a buffer layer of STO with 4-8 unit cells, between the SrMoO₃ film and the STO (or KTO) substrate. Such

buffer layer has been used for the growth of SrMoO₃ and EuMoO₃ by PLD^{9,10,22}. In this study, we firstly deposited SrTiO₃ using Sr and Ti under O₂ gas flow, and then we started the growth of SrMoO₃ films at the peak top of oscillation in RHEED for SrTiO₃ (Figs. 1(a) and (b)). The interval between each peak corresponds to one unit cell of SrMoO₃ (or SrTiO₃)²³. For substrates of SrTiO₃ and Nb-doped SrTiO₃, the oscillation amplitude gradually reduced after the growth of 10–15 unit cells of SrMoO₃ (Fig. 1(a)), while it retained almost constant in the case of the KTaO₃ substrate (Fig. 1(b)). For comparison, we present RHEED intensity profiles during the growth of the SrMoO₃ film on the non-buffered KTO substrate (Fig. 1(c)). It is seen that the RHEED intensity oscillation soon disappears when no buffer is used (Fig. 1(c)). The growth of 25–40 unit cells of SrMoO₃ (10–16 nm) was checked by the RHEED intensity oscillations or estimating time with the average interval of oscillation peaks or with the growth rates. Figures 1(d)–(f) display RHEED patterns at the end of the growth for the same samples in Figs.1(a)–(c), respectively. Streaky RHEED patterns ensure flat surface of the films (Figs.1(d)–(e)), while the spot-like (or slightly modulated) features are observed along with original streaks for the film without the buffer layer (Fig.1(f)), suggesting roughening of the film surface²⁴. We also used the so-called STEP substrate of SrTiO₃ with 100% TiO₂-terminated surface, but epitaxial growth was not possible in the current growth condition. The difference between the presence and absence of the buffer layer for the electrical conductance will be discussed in a later section.

Figures 2(a)–(b) show the out-of-plane θ - 2θ XRD patterns for the same samples in Figs. 1(a)–(c). Sharp peaks

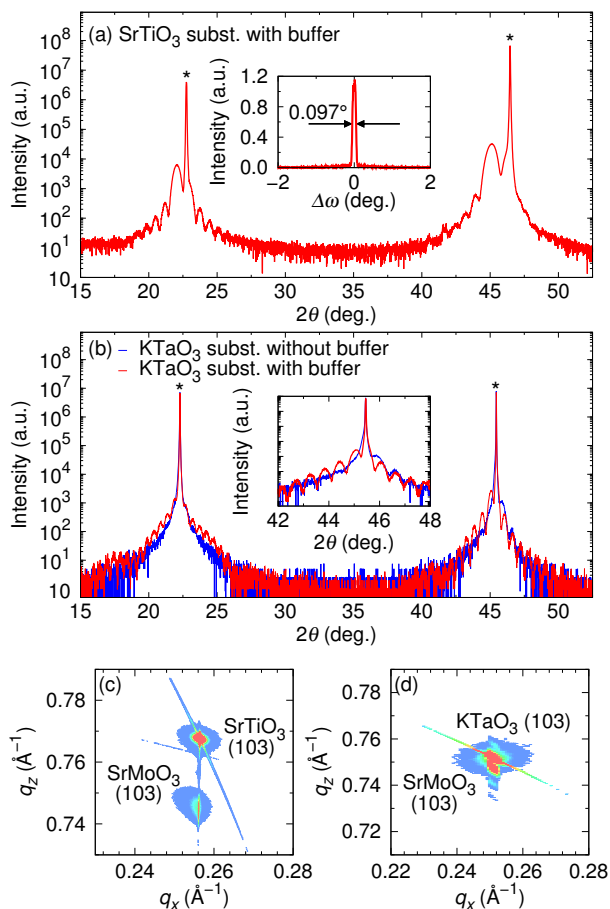


FIG. 2. Out-of-plane θ - 2θ XRD patterns of the films on (a) the STO substrate and (b) the KTO substrate. Data of the same samples of Figs. 1(a)-(c) are presented in (a)-(b). Substrate peaks are marked with an asterisk. The insets of (a) and (b) shows the rocking curve of the 001 peak around 22° , and the elongation of the 2θ scan around 45° , respectively. (c)-(d) X-ray reciprocal space mapping around the 103 reflection.

with distinct fringes are observed around $2\theta = 22^\circ$ and 45° for the SrMoO₃ film on the STO-buffered STO (S-STO) substrate (Fig. 2(a)), indicating excellent orientation and atomic scale smoothness of the interface between the substrate and the film. A similar tendency of the XRD profile and fringes is observed in the films on the STO-buffered KTO (S-KTO) and non-buffered substrates (Fig. 2(b)), where the XRD peaks of the films are overlapped with those of the KTO substrates. It is seen that fringes of the XRD spectrum of the SrMoO₃ film on the non-buffered KTO substrate are weakened (the inset of Fig. 2(b)), implying poorer quality of the film interface with the substrate. This result is consistent with the RHEED observation (Fig. 1(f)), suggesting island growth and its coalescence accompanied by the generation of grain boundaries and/or impurities²⁵. The film thickness estimated from the spacing of fringes is 11.3 nm, 15.6 nm, and 16 nm for the films on the S-

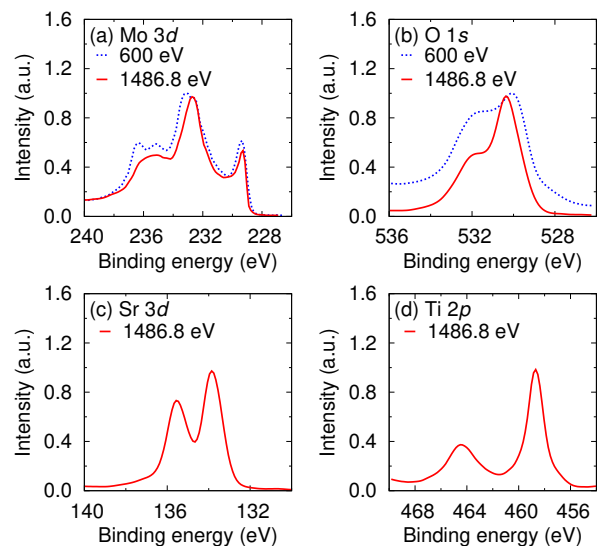


FIG. 3. Core-level x-ray photoemission spectra of a SrMoO₃ film for (a) Mo 3d, (b) O 1s, (c) Sr 3d and (d) Ti 2p. The Mo 3d and O 1s spectra were measured by both $h\nu = 600$ and 1486.8 eV in order to check the surface state. The Sr 3d and Ti 2p spectra were measured by $h\nu = 1486.8$ eV.

STO, S-KTO, and non-buffered KTO substrates, respectively. These values agree with the thickness estimated from the interval of RHEED oscillation peak and time as well as the growth rate. The rocking curve of the XRD peak around the 001 peak for the film on the STO substrate ($2\theta \simeq 22^\circ$) is $\Delta\omega = 0.097^\circ$ (inset of Fig. 2(a)). This value is slightly broader than that of SrMoO₃ films on the GdScO₃ substrate with PLD^{8,9}, which is probably because our film is thinner. An alternate possibility is a lattice mismatch between the bulk SrMoO₃ ($a = 3.975$ Å) and SrTiO₃ ($a = 3.905$ Å), leading to a strain effect. In fact, a pseudocubic lattice constant of GdScO₃ ($\bar{a} = 3.973$ Å)²⁶ is closer to that of bulk cubic SrMoO₃. The rocking curve of the (00l) peaks of the SrMoO₃ films on the KTO substrates was not measured due to the fact that the sample peaks are overlapped with the substrate peaks. Figure 2(c) and (d) show the reciprocal space mappings around the 103 peak of SrMoO₃ for the film on the S-STO and S-KTO substrates. The 103 peaks of the films are located near the same q_x value of the 103 peaks of the substrates, indicating a coherent growth of the target film, with an in-plane lattice parameter almost identical to that of the substrate. The lattice parameters of the SrMoO₃ film on the S-STO substrate are $a = 3.90$ Å, and $c = 4.02$ Å, meaning that the cell volume is reduced by about 3% relative to the bulk sample²¹. The reduced/expanded a/c axis is reasonable given the compressive strain from the SrTiO₃ substrate. The lattice parameters of the SrMoO₃ film on the S-KTO substrate are $a = 3.99$ Å (in-plane) and $c = 3.99$ Å (out of plane). The overall lattice expansion of the film about 1% in volume with respect to bulk SrMoO₃ may result

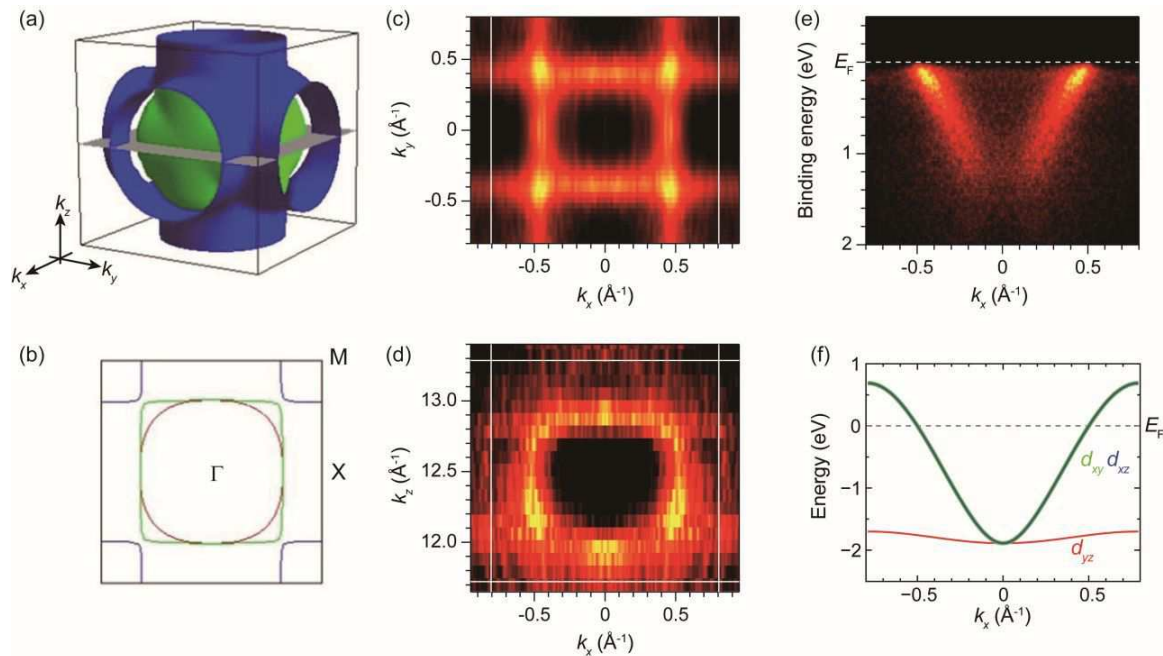


FIG. 4. (a) Fermi surfaces of non-magnetic cubic SrMoO₃. (b) Fermi-surface cross sections on the k_z (or k_y) plane. (c) Constant energy ARPES image of the SrMoO₃ film on the k_z plane. (d) Constant energy ARPES image of the SrMoO₃ film on the k_y plane. (e) ARPES intensity map along the $X-\Gamma-X$ direction. (f) Calculated band dispersions of SrMoO₃ along the $X-\Gamma-X$ direction.

from the tensile substrate strain which could also induces oxygen vacancies²⁷.

Core-level photoemission spectrum of the SrMoO₃ film provided evidence for the Mo⁴⁺ state associated with two sharp peaks at the binding energy of 229.3 eV and 232.6 eV for the photon energy of 1486.8 eV (Fig. 3(a)). A broad satellite was also observed next to the sharp peaks, which is likely Mo⁴⁺ 3*d* emission of unscreened final states^{9,10,28,29}. We also collected a spectrum at a lower photon energy (600 eV), which is more sensitive for the film near the surface, and observed additional features at 233.1 eV and 236.4 eV. These peaks are attributed to Mo⁶⁺ 3*d* emissions as observed in MoO₃^{12,28,29}, suggesting the oxidation of Mo around the interface with the topmost capping layer of STO (~ 0.4 nm). Note that the broad feature at about 235 eV cannot readily be explained by a simple component of Mo states; it may be due to plasmon satellite as discussed by Wadati *et al.*¹². The interface oxidations were also confirmed by O 1*s* spectra (Fig. 3(b)), with two prominent features at 530.2 eV and 532 eV. Since the contribution from the STO capping layer is expected to be about 20% for $h\nu = 1486.8$ eV³⁰, this additional 532 eV peak mainly comes from Mo⁶⁺ containing impurities around the SrMoO₃ film. The relative intensity at 532 eV (vs. 530.2 eV) increases when the photon energy of 600 eV is used. No influence of oxidation is seen in the Sr 3*d* spectrum with peaks for the Sr²⁺ state (Fig. 3(c)), implying the composition of Sr²⁺Mo⁴⁺O₃ in the most part of the

film. The peak positions of the Ti 2*p* spectrum from the STO capping layer are in good agreement with reported data^{9,31}, though the spectrum is slightly broader (Fig. 3(d)).

In order to investigate the electronic structure of the SrMoO₃ film, we performed ARPES measurements in the two-dimensional k space. Here one can ignore the contribution of Mo⁶⁺ in the surface to the obtained data near E_F , owing to its insulating d^0 state. The Fermi surface (FS) mapping on the k_x - k_y plane and the k_x - k_z plane (Figs. 4(c) and (d)), recorded with varying $h\nu$ from 500 to 700 eV, exhibits strong intensity with parallel-cross and ellipse patterns. These results can be reproduced computationally (see FS in Figs. 4(a) and (b)), and assure the high quality of the film (apart from Mo⁶⁺ in the surface). It is remarkable that in Fig. 4(e), a parabolic-like dispersion is clearly seen from ARPES spectra near E_F along the $X-\Gamma-X$ path (the cut in Fig. 4(c) for the k_x direction with $k_y = 0$). In the present experimental geometry, where p -polarized incident light and the analyzer slit are in the xz mirror plane of the sample, the d_{xz} band having even parity with respect to the xz mirror plane is observable, while the the d_{xy} and d_{yz} bands having odd parity are not³². These considerations led us to conclude that the observed dispersion originates from the d_{xz} -derived band, which is again supported by the band structures (Fig. 4(f)).

Figure 5 displays the temperature dependence of electrical resistivity ρ of SrMoO₃ films of thickness of about

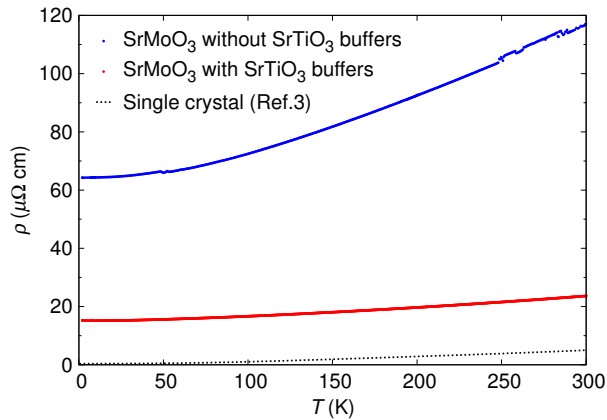


FIG. 5. Temperature dependence of ρ of the SrMoO₃ film on the KTaO₃ substrate with and without a SrTiO₃ buffer layer. ρ of a single crystalline sample³ is also compared.

16 nm on the KTaO₃ substrate with and without the SrTiO₃ buffer layer. Both films exhibit metallic temperature dependence but ρ of the film with the buffer layer is notably smaller. When the buffer layer is employed, the RT resistivity drops to 24 $\mu\Omega$ cm (from 117 $\mu\Omega$ cm without the buffer layer). This value is smaller than the reported values of films with similar thickness, 34 $\mu\Omega$ cm¹¹, but is five times larger than 5 $\mu\Omega$ cm for the bulk single crystal³. Here, the contribution from the STO buffer to the resistivity is negligible, since the stoichiometric sample of SrTiO₃ is a band insulator. It is also known that oxygen deficient samples SrTiO_{3- δ} show metallic conduction, but ρ is in the order

of 1 ~ 100 m Ω cm for lightly and heavily δ -doped (oxygen deficient) samples^{33,34}, which is $10^3 \sim 10^5$ times larger than that of SrMoO₃^{3,11}. The residual resistivity ratio RRR ($=\rho(300\text{ K})/\rho(2\text{ K})$) of the film with and without the buffer layer shows almost the same value of 1.7–1.8, implying that the crystallinity of both films is similar. It is thus considered that the larger electrical resistivity of the film without the buffer layer arises from extrinsic effect such as grain boundaries and surface/interface impurities, as suggested from the RHEED and XRD observations (Figs. 1 and 2). Further efforts are necessary to improve the transport properties of SrMoO₃ films, in conjunction with the clarification of the role of the presence and absence of the buffer layer for the amount of impurities with the Mo⁶⁺ state.

IV. CONCLUSION

We have succeeded in growing SrMoO₃ films using MBE growth technique. Introduction of SrTiO₃ buffer layer of 4–8 unit cells between the SrMoO₃ film and the (001)-oriented SrTiO₃ or KTaO₃ substrate improves the quality of the film, showing the five-times smaller resistivity than that of the film without the buffer layer. Clear observation of FS in ARPES measurements also ensures the high quality of the SrMoO₃ film grown by MBE.

ACKNOWLEDGEMENTS

This work was supported by CREST (JPMJCR1421) and JSPS KAKENHI Grants (No. 16H06439 and No. 17H04849).

¹ R. J. D. Tilley, *Perovskites: Structure-Property Relationships* (John Wiley & Sons, Ltd., USA, 2016).
² L. H. Brixner, *J. Inorg. Nucl. Chem.* **14**, 225 (1960).
³ I. Nagai, N. Shirakawa, S. Ikeda, R. Iwasaki, H. Nishimura, and M. Kosaka, *Applied Physics Letters* **87**, 024105 (2005).
⁴ A. P. Mackenzie, *Rep. Prog. Phys.* **80**, 032501 (2017).
⁵ T. Inukai and T. Murakami, *J. J. Appl. Phys.* **24**, 21 (1985).
⁶ H. Mizoguchi, N. Kitamura, K. Fukumi, T. Mihara, J. Nishii, M. Nakamura, N. Kikuchi, H. Hosono, and H. Kawazoe, *J. Appl. Phys.* **87**, 4617 (2000).
⁷ H. H. Wang, D. F. Cui, Y. L. Zhou, Z. H. Chen, F. Chen, T. Zhao, H. B. L. G. Z. Yanga, M. C. Xub, Y. C. Lanb, X. L. Chenb, H. J. Qianc, and F. Q. Liuc, *J. Cryst. Growth* **226**, 261 (2001).
⁸ A. Radetinac, K. S. Takahashi, L. Alff, M. Kawasaki, and Y. Tokura, *Appl. Phys. Express* **3**, 073003 (2010).
⁹ A. Radetinac, A. Mani, S. Melnyk, M. Nikfalazar, J. Ziegler, Y. Zheng, R. Jakoby, L. Alff, and P. Komissinskiy, *Appl. Phys. Lett.* **105**, 114108 (2014).
¹⁰ P. Salg, D. Walk, L. Zeinar, A. Radetinac, L. Molina-Luna, A. Zintler, R. Jakoby, H. Maune, P. Komissinskiy, and

L. Alff, *APL Mater.* **7**, 051107 (2019).
¹¹ A. Radetinac, J. Zimmermann, K. Hoyer, H. Zhang, P. Komissinskiy, and L. Alffa, *J. Appl. Phys.* **119**, 055302 (2016).
¹² H. Wadati, J. Mravlje, K. Yoshimatsu, H. Kumigashira, M. Oshima, T. Sugiyama, E. Ikenaga, A. Fujimori, A. Georges, A. Radetinac, K. S. Takahashi, M. Kawasaki, and Y. Tokura, *Phys. Rev. B* **90**, 205131 (2014).
¹³ D. G. Schlom, *APL Mater.* **3**, 062403 (2015).
¹⁴ D. Oka and T. Fukumura, *CrystEngComm* **19**, 2144 (2017).
¹⁵ H. H. Wang, G. Z. Yang, D. F. Cui, H. B. Lu, T. Zhao, F. Chen, Y. L. Zhou, and Z. H. Chen, *J. Vac. Sci. Tech. A* **19**, 930 (2001).
¹⁶ (), it has been reported that the value of the RT resistivity ρ_{RT} decreases from 34 $\mu\Omega$ cm to 27 $\mu\Omega$ cm with increasing the film thickness from 15 nm to 60 nm¹¹. This result implies the influence of the oxidized surface of SrMoO₃ films. Compared with samples with the same thickness, ρ_{RT} of our films in this study is 30% smaller than that of previous reports.

- ¹⁷ P. Giannozzi, S. Baroni, N. Bonini, M. Calandra, R. Car, C. Cavazzoni, D. Ceresoli, G. L. Chiarotti, M. Cococcioni, and I. Dabo, *Journal of Physics: Condensed Matter* **21**, 395502 (2009).
- ¹⁸ P. Giannozzi, O. Andreussi, T. Brumme, O. Bunau, M. B. Nardelli, M. Calandra, R. Car, C. Cavazzoni, D. Ceresoli, and M. Cococcioni, *Journal of Physics: Condensed Matter* **29**, 465901 (2017).
- ¹⁹ G. Kresse and D. Joubert, *Phys. Rev. B* **59**, 1758 (1999).
- ²⁰ J. P. Perdew, K. Burke, and M. Ernzerhof, *Phys. Rev. Lett.* **77**, 3865 (1996).
- ²¹ R. B. Macquart, B. J. Kennedy, and M. Avdeev, *J Solid State Chem.* **183**, 249 (2010).
- ²² Y. Kozuka, H. Seki, T. C. Fujita, S. Chakraverty, K. Yoshimatsu, H. Kumigashira, M. Oshima, M. S. Bahramy, R. Arita, and M. Kawasaki, *Chem. Mater.* **24**, 3746 (2012).
- ²³ T. Terashima, Y. Bando, K. Iijima, K. Yamamoto, K. Hirata, K. Hayashi, K. Kamigaki, and H. Terauchi, *Phys. Rev. Lett.* **65**, 2684 (1990).
- ²⁴ S. Hasegawa, “Reflection high-energy electron diffraction”, *Characterization of Materials*, ed., E. N. Kaufmann (Wiley, New York, 2012). p. 1925 – 1938.
- ²⁵ L. B. Freund and S. Suresh, *Thin Film Materials: Stress, Defect Formation and Surface Evolution* (Cambridge University Press, Cambridge, 2003).
- ²⁶ J. Schubert, O. Trithaveesak, A. Petraru, C. L. Jia, R. Uecker, P. Reiche, and D. G. Schlom, *Appl. Phys. Lett.* **82**, 3460 (2003).
- ²⁷ U. Aschauer, R. Pfenninger, S. M. Selbach, T. Grande, and N. A. Spaldin, *Phys. Rev. B* **88**, 054111 (2013).
- ²⁸ R. J. Colton, A. M. Guzman, and J. W. Rabalais, *J. Appl. Phys.* **49**, 409 (1978).
- ²⁹ D. O. Scanlon, G. W. Watson, D. J. Payne, G. R. Atkinson, R. G. Egdell, and D. S. L. Law, *J. Phys. Chem. C* **114**, 4636 (2010).
- ³⁰ (), using the QUASES-IMFP-TPP2M software³⁵, the inelastic mean free path (IMFP) of photoelectron from O 1s is about 2 nm in SrMoO₃ for $h\nu = 1486.8$ eV. With these IMFP and $h\nu$ values, we roughly estimated 20% (80%) contributions from SrTiO₃ (SrMoO₃) to the O 1s spectrum. We also obtained 15–18% contributions from SrTiO₃ to the Sr 3d spectrum, using the estimated IMFP of 2.3–2.5 nm and $h\nu = 1486.8$ eV.
- ³¹ C. D. Wagner, W. M. Riggs, L. E. Davis, and J. F. M. G. E. Muilenberg, *Handbook of x-ray photoelectron spectroscopy: a reference book of standard data for use in x-ray photoelectron spectroscopy* (Perkin-Elmer Co., USA, 1979).
- ³² R. Yukawa, S. Yamamoto, K. Ozawa, M. D’Angelo, M. Ogawa, M. G. Silly, F. Sirotti, and I. Matsuda, *Phys. Rev. B* **87**, 115314 (2013).
- ³³ X. Lin, G. Bridoux, A. Gourgout, G. Seyfarth, S. Kramer, M. Nardone, B. Fauque, and K. Behnia, *Phys. Rev. Lett.* **112**, 207002 (2014).
- ³⁴ W. Gong, H. Yun, Y. B. Ning, J. E. Greedan, W. R. Datars, and C. V. Stager, *J. Solid State Chem.* **90**, 320 (1991).
- ³⁵ S. Tanuma, C. J. Powell, and D. R. Penn, *Surf. Interf. Anal.* **21**, 165 (1994).